applied sciences

MDPI

Article

Study of the Internal Rebreaking Characteristics of Crushed Gangue in Mine Goaf during Compression

Peng Wen [1], Sen Han [1], Wenbing Guo [2,3], Weiqiang Yang [2,*] and Erhu Bai [2,3]

[1] School of Environment and Resource, Southwest University of Science and Technology, Mianyang 621010, China; wenpengcumt@126.com (P.W.); m18382723129@163.com (S.H.)
[2] School of Energy Science and Engineering, Henan Polytechnic University, Jiaozuo 454000, China; guowb@hpu.edu.cn (W.G.); baieh@hpu.edu.cn (E.B.)
[3] State Collaborative Innovation Center of Coal Work Safety and Clean-Efficiency Utilization, Jiaozuo 454000, China
* Correspondence: yangwq0222@163.com

Abstract: The deformation and re-crushing characteristics of different lithological caving crushed gangues in mine goaf directly affect the overburden strata movement, which significantly affects the surface subsidence of mining goaf. The effect of particle size on the re-crushing characteristics of different lithological caving crushed gangues in mine goaf is investigated in this study based on an innovative compression–AE (acoustic emission) measuring method. The results showed the following: (1) The compression deformation was divided into three stages: rapid, slow, and stable compaction. With the increase in axial pressure, the large particle skeletons were destroyed, medium particles were displaced and slid, and small particles filled the pores. (2) For singular lithologies, stress was positively correlated with pressure, and porosity was negatively correlated with stress. The composite sample was between the singular gangue samples. (3) The fractal dimension of crushed gangue samples was exponentially related to the proportion of gangue in singular and combined lithologies. (4) The cumulative AE count and energy of the combined lithological gangue samples were between those of the singular samples. The research results provide a theoretical foundation for further research into the characteristics of the overlying strata, surface movement, and safety management of the goaf.

Keywords: combination lithology; compaction characteristics; rebreaking characteristics; acoustic emission

check for updates

Citation: Wen, P.; Han, S.; Guo, W.; Yang, W.; Bai, E. Study of the Internal Rebreaking Characteristics of Crushed Gangue in Mine Goaf during Compression. *Appl. Sci.* **2024**, *14*, 1682. https://doi.org/10.3390/app14051682

Academic Editor: Stefano Invernizzi

Received: 13 December 2023
Revised: 7 February 2024
Accepted: 9 February 2024
Published: 20 February 2024

Copyright: © 2024 by the authors. Licensee MDPI, Basel, Switzerland. This article is an open access article distributed under the terms and conditions of the Creative Commons Attribution (CC BY) license (https://creativecommons.org/licenses/by/4.0/).

1. Introduction

Many coal mines in China have caused damage to the land, buildings, bodies of water, and other protected objects in mining areas [1–4]. At the same time, after the mining of coal seams, the overlying strata are deformed and damaged. In the overburden, many fissures are produced and a "two zone" or "three zone" failure pattern will be formed [5–8]. Layer by layer, the broken rock layer rises to the surface and serves as a force transmission beam [9]. The control of goaf conditions in underground mines directly affects the degree of surface subsidence. Many countries use tailing backfilling methods for treatment, not only treating tailings but also reducing surface subsidence. The compaction of crushed gangue in the caved zone, and its influence on the overlying strata and surface movement, has significant impact on and plays an important part in the formation of goaf conditions in underground mines and the control of surface subsidence [3,10,11]. Therefore, investigating the compaction characteristics of fractured rocks in mine goaf is vital for understanding the mechanism of overlying rock instability.

Numerous academics have investigated the compaction-induced deformation properties of crushed coal rock, which is crucial for the accurate porosity estimation of the mining goaf and safe and efficient production for coal mining [12]. Relatively early research was

conducted on the connection between coal gangue compaction properties and particle size distribution by Jiang et al. [13] and Ma et al. [14]. Huang et al. [15,16] revealed that the rock movement was regulated by the compactness of various gangue and fly ash filling bodies. Crushed particles under axial loading display a more complicated compression deformation process and pore structure evolution than intact coal and rock [17,18]. Yu et al. [19] discovered that more rock particles undergo re-crushing during compression the higher the power index n of the gradation. Liu et al. [20], using uniaxial compression tests on rocks, determined the link between the strain, compaction, and axial stress of crushed rock. The testing of cyclic uniaxial compression loading on sandstone samples was performed by Yang et al. [21], who also reported on the materials' deformation process during the loading cycle. Through testing, Zhou et al. [22] were able to determine the pattern of variation for parameters including the strain rate, Poisson's ratio, and the elastic modulus of sandstone. They discovered that the degree of rock damage caused a positive correlation between the pre-stress and the degree of sample fragmentation. Zhang et al. [23] established that the bearing capacity decreases with rising ambient humidity and, the higher the grading index, the faster the rate of change of the fragmentation rate. In terms of compaction characteristics, Liu et al. [24] found that the breaking rate of crushed rock gradually increased with the increase in the intermediate principal stress ratio during true triaxial compression. Li et al. [25,26] conducted compression tests using a unique large diameter compression steel chamber and an SANS material testing machine and compared and analyzed the relationship between the deformation modulus and compactness, resulting in a linear growth relationship between the deformation modulus and the stress of coal gangue samples. Zhang et al. [27–29] unanimously discovered that the compression characteristics of crushed media were affected significantly by the axial loading stress and rock type.

To investigate the tiny internal deformation and re-crushing law of crushed coal rock, Wu et al. [30] used PFC2D-based numerical simulation software to study the mechanical bearing characteristics, particle breakage, force chain structure, and other micro aspects of different particle-sized gravel. Wang and Li [31] conducted a quantitative analysis of the impact of internal particle re-crushing on macro deformation using the CT reconstruction approach. Cheng et al. [32] built a discrete element model of cemented calcareous sand to examine the microscopic mechanical behavior under two-dimensional shear circumstances. Moreover, a number of researchers have attempted to investigate the evolutionary properties of the particle skeleton and porosity structure of crushed coal rocks using three-dimensional (3D) computed tomography (CT) reconstruction. After analyzing CT scan data, Yang et al. [33] computed the volume porosity and pore size distribution. Feng et al. [34] quantitatively characterized coal particles with layered re-crushing behaviors using a self-designed CT visual compacting device.

Acoustic emission (AE), a non-destructive monitoring method, offers important data on the dynamic degradation of coal rocks and material quality detection [35–37]. Mao et al., Michlmayr et al., and Johnson et al. [38–41] detected them during the shearing process of spherical granular glass beads, and analyzed the typical frequency range of AE during the shearing process. Feng et al. [42,43] investigated the effect of particle size on the re-crushing characteristics based on an innovative compression–AE (acoustic emission) positioning method. The result showed that the deformation and re-crushing characteristics of the crushed coal and rock directly affected the porosity and permeability distribution of the mining goaf and overburden strata movement. Li [44,45] conducted an AE experimental study on crushed gangue under different loading conditions and analyzed the corresponding relationship between AE parameters and strain–stress curves. According to Xin et al. [46], there were notable differences in each compression stage of the crushed coal rock, as indicated by the cumulative AE counts. The maximum and cumulative AE energies were found to grow continuously with the loading rate by Qin et al. [47]. The effects of particle gradation and loading circumstances on the crushed rock's AE parameters during compression were also reported in other investigations [48].

The research described above offers a wealth of resources for comprehending how lithology, gradation, particle size, and loading rate affect the properties of crushed rock and coal during compression. The main focus is on the compaction of gangue and the comparison of the compaction characteristics of a single particle size and crushed rocks of the same lithology. Studies on the compaction characteristics of combined lithology and mixed particle sizes are rare, while studies on crushed gangue in goaf are mostly composed of gangue formed after two or more kinds of crushed lithology. The research on AE characteristics mainly focuses on the topic of crushed coal rock, with studies on combined lithology crushed rocks in goaf being less common. The evolution law of the micro and macro structure of combined lithology crushed rocks in mine goaf and the mechanism of pressure bearing deformation are still unclear. In light of this, this paper conducted a confined compression AE monitoring test of mixed particle sizes and combined lithology through an independently designed gravel compression device. The compression deformation characteristics of crushed rocks in mine goaf with different single and combined lithologies will be touched upon, as well as the energy and fracture evolution law of the compaction process of crushed rocks in mine goaf. The pressure bearing deformation mechanism of crushed rocks in mine goaf from the micro level will be revealed, providing a basis for the study of overburden and surface movement.

2. Materials and Methods

2.1. Test Materials

Many physical and numerical simulations and field monitoring all show that from the boundary between the caved zone and the fracture zone to the direction of the floor of the working face, the degree of fragmentation of the caved gangue gradually increases, and the thickness of the caved gangue gradually decreases to a certain extent. The lithological distribution of caved gangues is the same as that of the direct roof of the coal seam, generally including at least two kinds of lithological gangues. The gangues in mine goaf have two characteristics: (1) the particle size of the gangue increases from bottom to top, and it is not a single particle size distribution, but a combined one; (2) the lithology of the caved zone is not a single form of lithology, but a combined one, as shown in Figure 1.

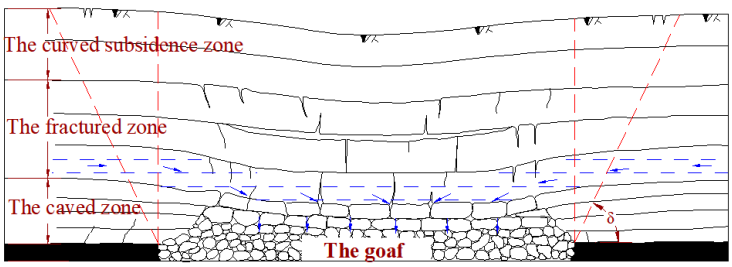


Figure 1. Schematic diagram of "three vertical zones" of overlying gangue in longwall cave mining.

The crushed particle size came from the complete caved zone gangue in the longwall goaf of a mine. The maximum thickness of the caved zone was about 20 m, and the container was prepared to contain a 200 mm high crushed gangue. Then, the geometric similarity ratio, αl, was 1:100. The maximum thickness of the gangue in the caved zone was 4.7 m. According to αl, the maximum particle size of the compaction test sample was 47 mm, the maximum particle size was 45 mm, and the different crushed particle sizes were 5–15 mm, 15–25 mm, 25–35 mm, and 35–45 mm.

2.2. Testing of Physical and Mechanical Parameters of Crushed Gangue

As shown in Table 1, the recovered bulk gangue sample was taken as the standard gangue sample, and the mechanical property parameters of the two samples, sandstone and sandy mudstone, were measured.

Table 1. Physical and mechanical parameters of crushed gangue in caved zone.

Lithology	Compressive Strength/MPa	Cohesion/MPa	Tensile Strength/MPa	Elastic Modulus/GPa	Internal Friction Angle/(°)
Sandstone	67.29	28.65	3.28	23.02	37.1
Sandy mudstone	38.25	3.99	0.97	9.5	33.82

2.3. Test System

Manual crushing was conducted in the laboratory, and the gangue was crushed according to the particle size. The samples were sealed to protect the gangue from weathering. The gangue samples were sieved with a round hole grading screen (Figure 2) to obtain the four samples with particle sizes of 5~15 mm, 15~25 mm, 25~35 mm, and 35~45 mm. The four samples with different particle sizes were mixed to an equal ratio to obtain two single mixed-particle-size loose gangue samples, and then these were combined in equal volumes to obtain combined lithology gangue samples (Figure 3). We took out the compacted sample and then screened and weighed it again.

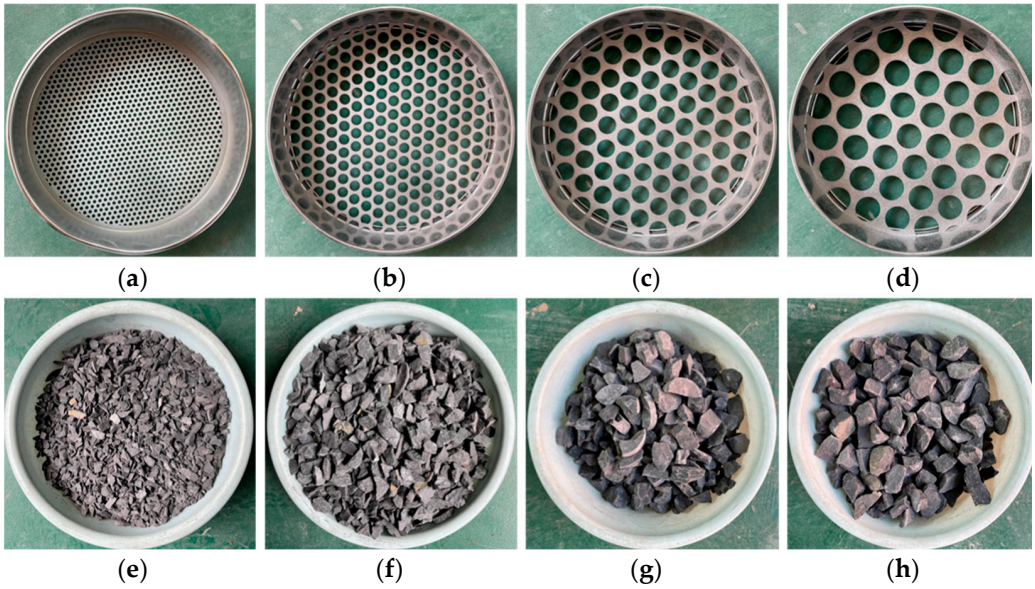


Figure 2. Round hole sieves of different sizes: (**a**) 15 mm; (**b**) 25 mm; (**c**) 35 mm; (**d**) 45 mm. Gangue of different sizes: (**e**) 5~15 mm; (**f**) 15~25 mm; (**g**) 25~35 mm; (**h**) 35~45 mm.

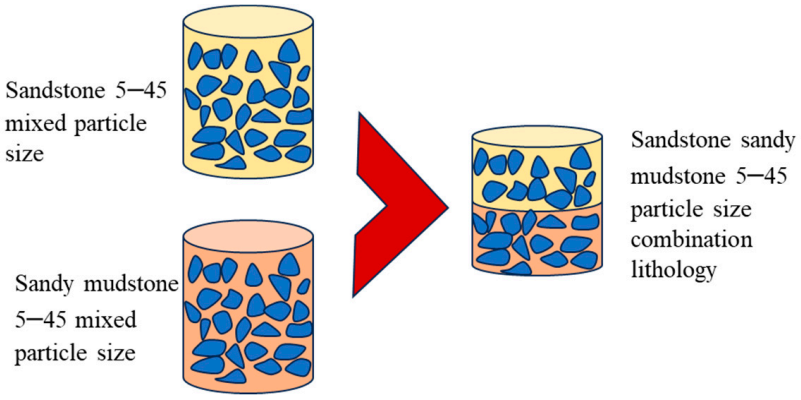


Figure 3. Schematic diagram of combined particle size and lithology.

The prepared loose gangue sample was placed into a cylinder with an inner diameter of 175 mm. The cylinder on an electro-hydraulic servo universal testing machine was placed

on top, and the sample was compressed. The self-designed broken rock–coal compression device, which is made of a high-strength steel alloy, can provide the test conditions for axial loading and hoop displacement constraints. In this test, the loading rate of the electro-hydraulic servo universal testing machine was 1 KN/s. The loading ended when the stress reached 25 MPa, and the loading height was 200 mm. The test apparatus is shown in Figure 4.

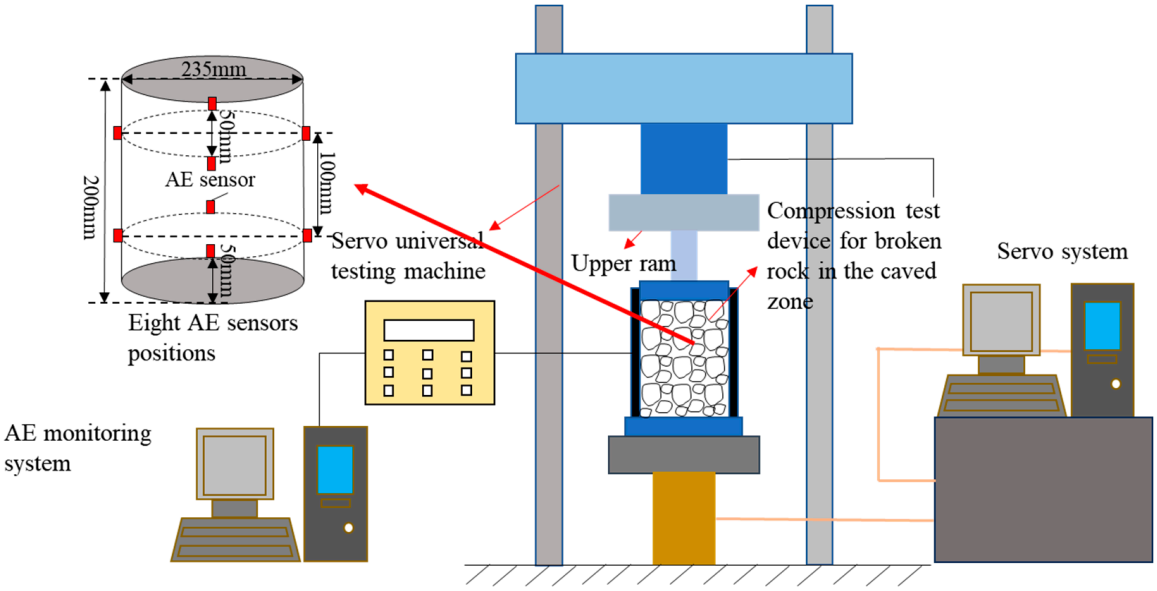


Figure 4. Schematic of testing system for caving crushed gangues of mine goaf.

The sampling frequency of this test system was 1MSPS, and the pre amplifier type was 40 dB. After re-adjustment, the fixed threshold value of the AE threshold was set to 40 dB and the surrounding noise was effectively shielded. Therefore, in this experiment, the AE threshold was set to 40 dB. The AE probe used in the test was Nano30, and its spatial layout is shown in Figure 4.

The corresponding sampling frequency of the probe was 20–200 KHz. The acquisition and processing software was AE win for PCI-2, which is included in the AE acquisition system. In order to ensure a good coupling effect during the test, the following measures were taken: (1) eight probes were used for AE monitoring; (2) the couplant was applied evenly to the surface of the probe, and the probe was stuck to the wall of the test cylinder with insulating tape and pressed firmly; and (3) a constant initial loading stress of 100 N was applied. To properly reduce the amount of AE data processing, the test did not consider the friction between the steel column of the compaction equipment and the mold.

3. Results

3.1. Confined Compression Deformation Characteristics of Fractured Gangues with Different Lithologies

3.1.1. Time-Strain

The strain times of sandstone, sandy mudstone, and a combination of both were recorded during compression, and the strain time change curves of all three crushed gangues were taken (Figure 5).

It can be seen from Figure 4 that in less than 50 s, the strain curves of the individual and combined lithological gangue samples showed a dramatic upward trend. After that, the three curves separated and showed different change characteristics. In the strain-time curve of sandy mudstone, the strain rose for the longest time and the largest strain was produced. Conversely, the sandstone produced the smallest strain. The lithology of the sandstone–sandy mudstone was a combination of the two and closer to the sandstone strain. After the initial rise in the three curves, all showed the characteristics of increasing

strain with time, rising sharply first and then with a gentle increase. The results suggested that the softer the gangue, the more dramatic the preliminary growth rate of the crushed gangue's strain, and the greater the final strain value reached at the end.

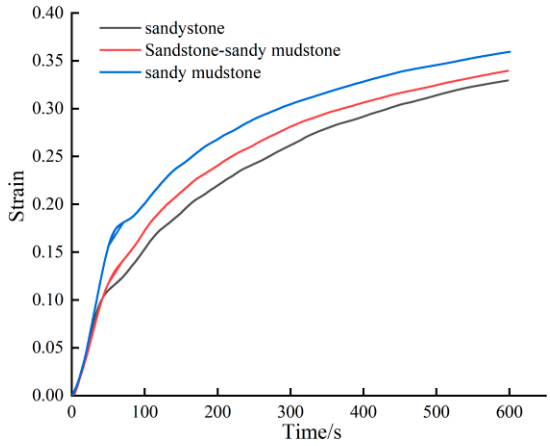


Figure 5. Strain-time curves of sandstone, sandy mudstone, and composite lithological crushed gangue samples during confined compression.

3.1.2. Stress–Strain

The stress and strain data during the compression of crushed gangue samples were recorded, and the stress–strain curves of sandstone, sandy mudstone, and a combination of both under confined compression were obtained (Figure 6).

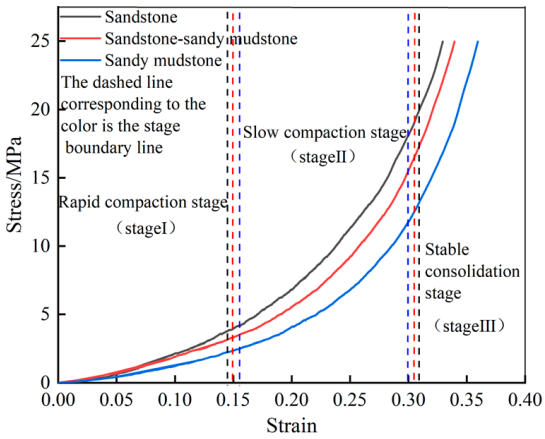


Figure 6. Stress–strain curves of sandstone, sandy mudstone, and composite crushed gangue samples during confined compression.

The following can be seen from Figure 6:

(a) The stress and strain of the crushed singular gangues and a combination of both were nonlinear during confined compression. As the strain increased, the axial stress increased steadily, while the strain growth rate decreased toward the end. However, in different stress stages, the variation in the strain was different. According to the evolution process of the slope change rate of the stress–strain curve of fractured gangue samples, the compaction deformation process of fractured gangue samples was divided into three stages:

(I) The rapid compaction stage.
(II) The slow compaction stage.
(III) The stable compaction stage.

Specifically, in Stage I, the crushed gangue was in a loose state, with many voids inside the crushed gangue, and the overall bearing capacity was very weak. The block

was extremely prone to deformation under axial pressure. In Stage II, the pores between crushed gangue blocks in mine goaf were gradually filled with crushed blocks as the axial stress increased, their resistance gradually increased, they were not prone to deformation after being stressed, and the strain growth rate gradually decreased. The boundary between Stage I and Stage II gradually shifted to the right as the elastic modulus of the lithology decreased; in Stage III, the blocks mainly meshed with each other at the point of contact. As the stress continued to increase, the strain value decreased due to the sliding, fracturing, and structural reorganization between the blocks. The larger the block particle size, the smaller the strain value, and the longer the duration. The pores between the blocks were filled by the crushed blocks. As the stress increased, the pores between the blocks decreased, and the blocks were gradually compacted to form a more stable overall structure. The strain curve gradually trended to a constant value. The boundary between Stages II and III gradually shifted to the right as the strength of the original gangue increased.

(b) The compression deformation characteristics of different crushed gangue samples varied. In the rapid compaction stage, the strain curves of single and combined lithologies were close. In the slow compaction stage, the strain curves of single and combined lithologies gradually separated. Under the same stress conditions, the strain of sandy mudstone was greater than that of the combination and that of sandstone. In the stable compaction stage, the strain of the confined compaction of crushed single and combined lithological gangues gradually increased, and the increase amplitude gradually decreased. After basic compaction, the strain of crushed sandstone was 0.33, that of the composite was 0.34, and that of sandy mudstone was 0.36. This indicated that the combined lithology of fractured sandstone and sandy mudstone improved its overall strength compared to a single lithology of sandy mudstone, changing the compaction characteristics of sandy mudstone to a certain extent and affecting the evolution process of sandy mudstone strain with stress.

(c) The strength values obtained in lateral compression tests for crushed gangue samples with higher hard crushed gangue content are also higher than those of gangue samples with lower hard gangue contents. Under lateral compression conditions, the compression deformation of the crushed gangue combination samples in goaf will decrease with an increase in the hard crushed gangue content. The aforementioned occurrence suggests that the structural properties of the composite gangue sample alter as the amount of hard crushed gangue rises. The crushed gangue in the sample will come into local mutual touch when the amount of hard crushed gangue grows to a specific point. The formation of a stable crushed gangue skeleton between the crushed gangue under lateral compression conditions increases the compressive strength of the composite gangue sample.

In conclusion, the strength of various crushed gangue types and the friction strength between them make up the majority of the strength of composite rock samples. The percentage of crushed gangue in various rock types and the lithology of the crushed gangue affect how much of an influence these two strength composition elements have on the overall strength of composite gangue samples. In combination lithology, the proportion of weak gangue samples is comparatively low, and the blocks are closely spaced to form the combination's framework. The spaces created between the massive pieces that make up the framework are partially filled in by small blocks. At this point, the biting force and friction force produced between the blocks are what primarily determine the macroscopic mechanical strength. The total strength mostly depends on the weak crushed gangue when there is less hard crushed gangue present. The block's existence barely influences the macro-scopic deformation and failure properties of the material.

3.1.3. Fractal Dimension

Many studies have shown that the particle size distribution of crushed gangue mass has a fractal structure. Fractal theory is widely used in the study of particle size distribution and the grading evolution characteristics of crushed gangue, which can comprehensively reflect the particle size distribution and fragmentation of crushed gangue before and after

loading [49]. The fractal dimension, expressed by D, is the representation of the complexity of the composition of a material and how it is self-organized. Under the action of a certain stress level, the particles in the crushed gangue sample move and slide, which changes its spatial arrangement and pore distribution. Because the cylinder used in the test had a large stiffness, the radial deformation of crushed particles was not considered in the loading process [50]. According to fractal theory in gangue crushing, the total mass of the crushed gangue is set as M_t, where the mass of particles smaller than the particle size di is $M_1(d_i)$, and the mass of particles larger than the particle size d_i is $M_2(d_i)$, where

$$M_t = M_1(d_i) + M_2(d_i) \tag{1}$$

The relationship between the volume V and the fractal dimension D of the fractured gangue in mine goaf is as follows:

$$V = C_v \left[1 - \left(\frac{d_i}{\lambda_v} \right)^{3-D} \right] \tag{2}$$

where C_v and λ_V are constants, and their size depends on the shape and distribution of the crushed gangue particle size.

According to Tyler and Wheatcraft's assumptions [51], if the density of each particle in the crushed gangue is the same, then

$$M_2(d_i) = \rho C_v \left[1 - \left(\frac{d_i}{\lambda_v} \right)^{3-D} \right] \tag{3}$$

From the above formula, when $d_i = 0$, there is

$$M_t = M_2(d_i) = \rho C_v \tag{4}$$

When $d_i = d_{\max}$ and $M_2(d_{\max}) = 0$, substituting Equation (3), we can obtain

$$\lambda_v = d_{\max} \tag{5}$$

From Formula (2) to Formula (6), the fractal relationship between the particle quality and particle size of crushed gangue can be obtained:

$$M_1(d_i)/M_t = [1 - M_2(d_i)]/M_t = (d_i/d_{\max})^{3-D} \tag{6}$$

The logarithm of the two sides of the equation can also be obtained:

$$\lg[M_1(d_i)/M_t] = (3 - D)\lg(d_i/d_{\max}) = k\lg(d_i/d_{\max}) \tag{7}$$

The relationship between the linear slope and fractal dimension is seen from Equation (8). The crushed gangues before and after compaction were screened and weighed. The logarithmic relationship between the mass ratio and particle size ratio was calculated according to Equation (8).

The different combinations of crushed gangue were graded by particle size. All gangue samples were sieved to the particle size ranges of 0~2, 2~5, 5~10, 10~15, 15~20, 20~25, 25~30, 30~35, and 35~40. The gangue samples in each particle size range were weighed and the mass proportion was calculated. Each particle size range contained sandstone and sandy mudstone. The gangue samples of single lithology and combined lithology after crushing were compared. The proportion of sandy mudstone in the large range (35~40 mm) gradually decreased after compression. It further showed that the high-strength gangue block was mainly skeleton-bearing, while the low-intensity gangue block was mainly pore-filling for the combined gangue sample. According to the gradient of the linear equation and the fractal dimension, the fractal dimension of single and combined gangues under

pressure was calculated, as shown in Figure 7 and Table 2. The compaction, crushing, and rescreening processes of crushed gangue samples from mine goaf are shown in Figure 8. The fractal dimension, D, of different lithologies was 2.277~2.349, and the correlation coefficient was above 0.98.

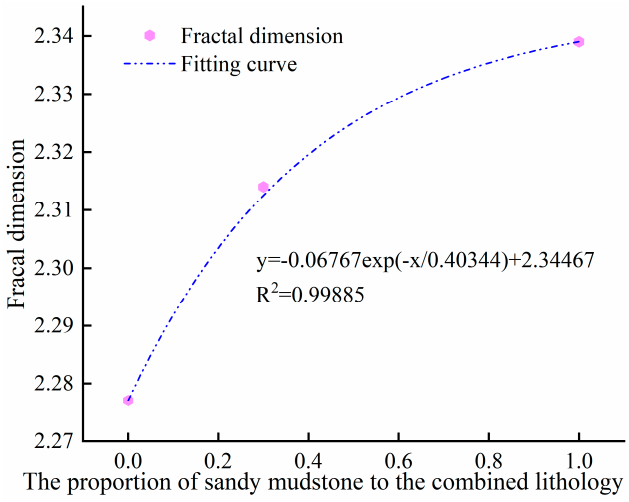


Figure 7. Relationship between fractal dimension and different lithological ratios.

Table 2. Particle size composition and fractal dimension of different single and combined lithology samples after compression.

Initial Particle Size	Crushed Gangue Mass						Correlation Coefficient	Fractal Dimension
	15~25 mm							
after compaction	0~2 mm	2~5 mm	5~10 mm	10~15 mm	15~20 mm	20~25 mm		
sandstone proportion/%	15.53	9.25	21.85	19.1	19.68	14.59	0.985	2.237
sandstone–sandy mudstone proportion/%	16.9	10.42	20.37	23.27	18.27	10.77	0.986	2.265
sandy mudstone proportion/%	20.47	11.25	23	16.78	18.52	9.97	0.99	2.349



Figure 8. Diagram of compaction, crushing, and rescreening of crushed gangue samples in goaf.

Figure 7 shows that the fractal dimension increases exponentially with the variation in different lithologies. The fitted result is

$$y = -0.06767 \exp(-x/0.40344) + 2.34467$$
$$R^2 = 0.99885$$

In the process of loading and compression, the breakup of the composite gangue samples increased with the increase in sandy mudstone, with the rate gradually decreasing. This was due to the small proportion of sandy mudstone effectively filling the ground pores between sandstone blocks after fracturing, which improved the structural stability. As the proportion of sandy mudstone continues to increase, the stability of the formed framework structure continues to decrease, and after compression, it will enter a cycle of "instability fracture recombination stability re instability".

3.2. AE Characteristics and Analysis of Crushed Gangue Compaction

3.2.1. Evolution of AE Parameters during Axial Compression

During the compression of the crushed gangue in the caved zone, the fracture of blocks and the friction between them produced AE signals. The AE strain time, ring count, and cumulative ring count curves for singular and combination crushed gangues during compression are shown in Figures 9–11. The AE parameter evolution properties are quite consistent with the three stages of stress–strain curves.

The following can be seen from Figures 9–11:

(a) The AE ring count and cumulative energy of the crushed sandstone, sandy mudstone, and sandstone–sandy mudstone combination gangue samples showed different variation characteristics at different strain stages. Their evolution law with time corresponded to the three stages of compaction characteristic tests. The AE ringing count and the evolution law of energy with time were used to characterize the different stages of the axial compression of crushed gangue samples under lateral constraint: In the sliding flow deformation stage of the crushed gangue sample (the strain was 0~0.1), the AE ring count, cumulative ring count, energy, and cumulative energy all showed a trend of rapid increase. With the increase in stress, the ring count and energy decreased sharply, and the rate of the cumulative count and cumulative energy tended to increase gently; when the crushed gangue entered the fracturing deformation filling stage (the strain was 0.1~0.25), the AE ring count and energy increased rapidly after the previous stage, and the cumulative ring count and energy showed an upward trend. In the compression elastic deformation stage of crushed gangue samples (where the strain was greater than 0.25), the AE ring count and energy showed a gradual decrease with continuous loading, while the cumulative AE count and cumulative energy curve increased gradually, and the late compression period showed a nearly linear growth.

(b) The cumulative ringing count of crushed sandstone was 1.1×10^5 and the cumulative energy was 28×10^6 J; the cumulative ringing count of crushed sandy mudstone was 9.7×10^5 and the cumulative energy was 92×10^6 J; the cumulative ringing count of a combination of crushed sandstone and sandy mudstone was 3.2×10^5 and the cumulative energy was 49×10^6 J. The cumulative ringing count of crushed sandy mudstone > the cumulative ringing count of crushed combination lithology > the cumulative ringing count of crushed sandstone and the cumulative energy of crushed sandy mudstone > the cumulative energy of crushed combination lithology > the cumulative energy of crushed sandstone.

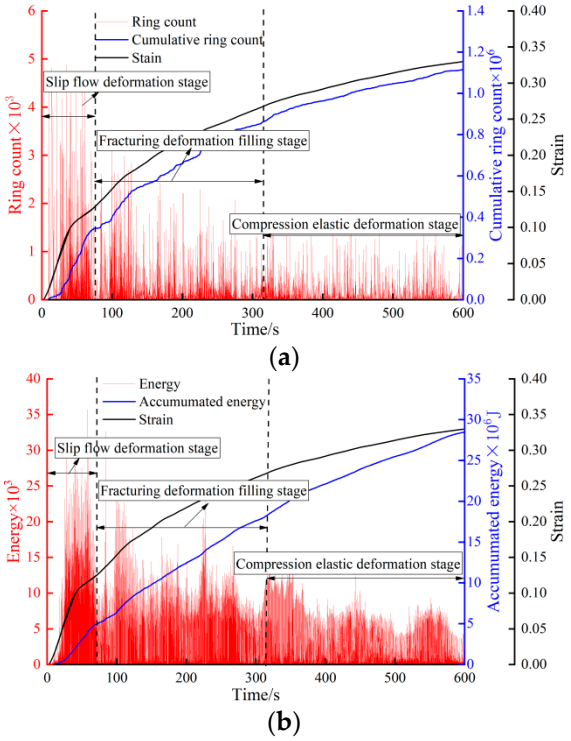


Figure 9. AE parameter curves of crushed sandstone. (**a**) AE ring count–cumulative ring count–strain-time. (**b**) AE energy–cumulative energy–strain–time.

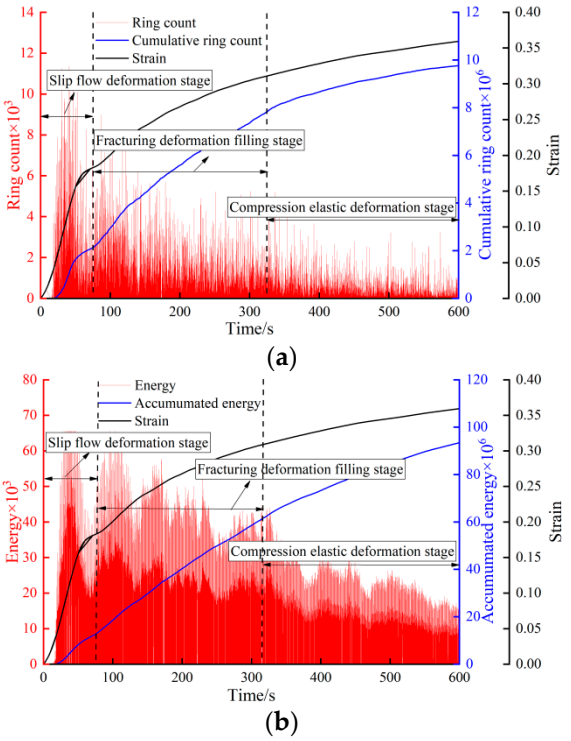


Figure 10. AE parameter curves of crushed sandy mudstone. (**a**) AE ring count–cumulative ring count–strain-time. (**b**) AE energy–cumulative energy–strain–time.

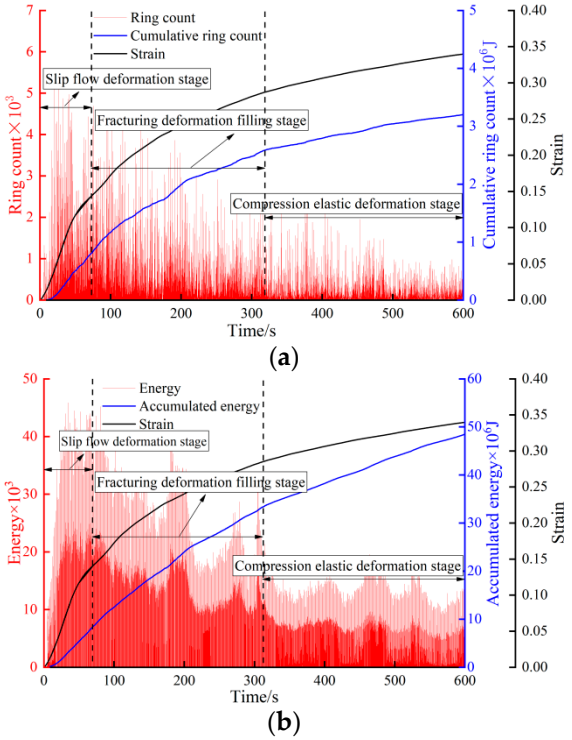


Figure 11. AE parameter curves of crushed sandstone and sandy mudstone. (**a**) AE ring count–cumulative ring count–strain-time. (**b**) AE energy–cumulative energy–strain-time.

3.2.2. Analysis of AE of Crushed Gangue Compaction Deformation

The number of AE ringing counts and energy can represent the number of crushed gangue samples. The AE characteristic curves of the sandstone, sandy mudstone and sandstone–sandy mudstone combination are shown in Figure 12.

The following can be seen from Figure 12:

(a) In the sliding flow deformation stage (which corresponded to the rapid compaction stage), the particles overcame the friction between them under the axial pressure to produce a wide range of dislocations and sliding. The pores between the blocks were compressed, the blocks and the crushed ones showed the adjustment of the contact state and the rapid closure of the interspace between them, the contact was relatively dense, the deformation speed was fast, the ringing count showed a significant increase, and the cumulative ringing count increased sharply. With the increase in axial stress, the gap between the crushed blocks continued to be filled and closed, and the blocks continued to rotate and move. During this period, the crushed gangue sample blocks formed a relatively dense skeleton as edges and corners met. The ring count decreased sharply, and the cumulative ring count increased slowly. Throughout the whole stage, there were crushed AE signals caused by a small number of irregular block corner breakages as well as friction AE signals caused by rotation, friction, and dislocation between the particles. Overall, the AE counts in this stage were relatively small.

(b) In the fracturing deformation filling stage (which corresponded to the slow compaction stage), the crushed blocks formed a combination with a relatively dense skeleton structure compared to that in the previous stage, with a slightly improved deformation resistance. Compared to the slip flow deformation stage, with the increase in stress, the AE count and energy generated by fracturing and crushing between the blocks, as well as the frictional AE count and energy caused by the denser skeleton, all gradually increased. At the initial stage of gangue block fracturing deformation and filling, the growth trend of the AE count was gentle, and as the axial stress increased, the cumulative AE count and energy curves showed a “convex” growth trend before being flattened.

(c) In the compaction elastic deformation stage (which corresponded to the stable consolidation stage), the crushed sandstone gangue sample block assembly had a "strain enhanced" skeleton structure, with relatively stronger deformation resistance than before, due to the stress in the early fracturing, deformation, and filling stages. In this stage, the work performed by the universal servo machine was converted into particle crushing and friction energy consumption, and the total amount of energy consumption decreased as the axial stress increased. Therefore, the whole AE cumulative count curve presented a convergent growth trend, as did the strain curve.

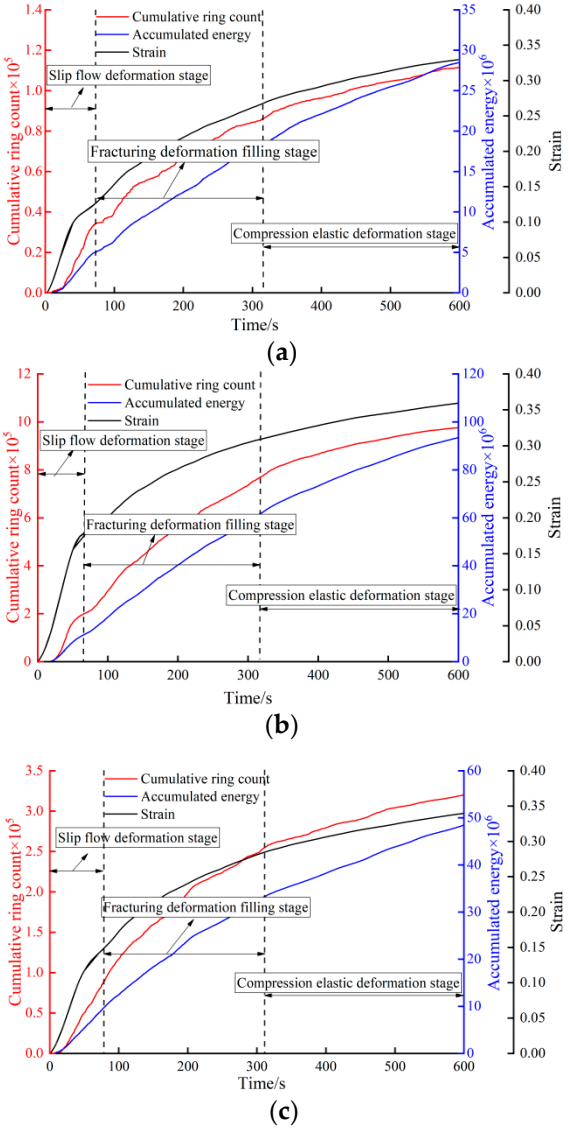


Figure 12. AE characteristics of sandstone, sandy mudstone, and sandstone–sandy mudstone crushed gangue samples during confined compression. (**a**) Sandstone. (**b**) AE energy–cumulative energy–strain-time. (**c**) Sandstone–sandy mudstone.

In conclusion, as the stress increased, the evolution characteristics of the AE of singular and combined crushed gangues in the caved zone showed a stage change and similar evolution laws. The evolution process of AE corresponded to the compaction process of the same samples.

4. Discussion

By comparing the strain conditions of different lithologies at the same time, we found that the softer the lithology, the faster the deformation rate of the overburden in the rising stage. In actual mining work, if the lithology of the overburden in the goaf is relatively soft, there may be significant residual deformation in the surface subsidence area in the early stage after the mining work is completed. Due to the faster compaction and maximum subsidence of this type of crushed gangues, the surface may reach a stable state faster. In addition, based on the analysis of stress and strain in different lithologies, if there is a hard interaction in the lithology of crushed gangues in goaf, their structural performance will be improved. Therefore, in goaf with harder gangue characteristics, the potential residual settlement in the goaf is greater, and we need to pay special attention to reinforcement treatment. These views are consistent with existing research findings [9,52].

The experimental results that were obtained are limited to the laboratory level and do not demonstrate a significant correlation with the compaction properties of the rock layers found on the site. However, there has not been much thought given to how water affects the process of compaction in cracked rocks. These represent the research constraints of this study and will be the main subject of my upcoming research.

The AE equipment used in the paper is a precision instrument, especially the AE probe, which is a vulnerable component and is only suitable for indoor testing. Through this research method and means, the compaction characteristics of small-sized fractured gangues sampled on site can be obtained based on the existing literature in the laboratory. Through similarity ratios, the failure law of overlying gangues in a large-sized goaf on site can be preliminarily determined. For on-site in situ monitoring, methods similar to the principles of AE equipment, such as wave velocity testing, shear wave testing, and seismic wave testing, can be used to obtain the movement and failure patterns of fractured gangues in the goaf. The monitoring cost is higher than that with commonly used monitoring methods such as RTK and total station, which will also be my future research focus.

5. Conclusions

(1) Under the condition of confined compression, the change curve of the axial strain of the crushed gangue sample in the caved zone with time showed a straight upward trend at the beginning of the test, which increased with time, showing a sharp rise at first before slowing at the end. The softer the lithology, the greater the initial rate of growth, and the greater the final strain value reached at the end of the test.

(2) The stress–strain curves of crushed gangues with different lithologies in the caved zone showed nonlinear growth. The difference was that the lower the strength of the gangue sample, the slower the initial rise of the curve, and the greater the final strain. The stress–strain curves showed typical characteristics, which were divided into the rapid compaction stage, slow compaction stage, and stable compaction stage. The strain of the combined samples were somewhere between those of the individual samples.

(3) In confined compression, the AE characteristics of crushed gangue were different at different deformation stages. Based on the AE test, the compaction process was divided into the sliding flow deformation stage, fracturing deformation filling stage, and compaction elastic deformation stage, corresponding to the stress and strain in the compression of the samples. The failures of the large particle skeleton, the sliding flow of medium particles, and the filling of pores by small particles were the main reasons for the compression deformation of crushed gangue samples, respectively.

(4) There was a positive correlation between the fractal dimension and the proportion of gangue samples with singular and combined lithologies, with the fitting degree above 0.98. Based on the compaction characteristics of crushed gangue samples and AE tests, the crushing stage characteristics of crushed gangue during compaction were summarized.

Author Contributions: Conceptualization, P.W., W.G. and W.Y.; methodology, W.G., E.B. and W.Y; software, P.W., W.Y. and S.H.; validation, P.W. and W.G.; formal analysis, P.W. and W.Y.; investigation, P.W., W.Y. and S.H.; data curation, P.W. and S.H.; writing—original draft preparation, P.W. and W.Y.; writing—review and editing, P.W., W.G. and W.Y.; supervision, W.G. All authors have read and agreed to the published version of the manuscript.

Funding: This research was funded by the Key Project of the National Natural Science Foundation of China (U21A20108, U1810203); the National Natural Science Foundation of China (52104127, 52174108, 51974105); the Henan Science and Technology Research Project (212102310399, 222102320058); the Project of Science and Technology Innovation Leading Talent in Central Plains (24200510012); the Henan Excellent Youth Science Foundation (222300420045); the Program for Science & Technology Innovation Talents in Universities of Henan Province (21HASTIT024); the scientific and technological innovation research team of Henan Polytechnic University (T2021-5); the Key Scientific Research Projects of Colleges and Universities in Henan Province (21A440003); and the Research fund of Henan Key Laboratory for Green and Efficient Mining & Comprehensive Utilization of Mineral Resources (Henan Polytechnic University) (KCF202002).

Institutional Review Board Statement: Not applicable.

Informed Consent Statement: Not applicable.

Data Availability Statement: The data used to support the findings of this study are included within the article.

Acknowledgments: This research was financially supported by the contents in the fundings. The authors thank the anonymous reviewers for their careful work and thoughtful suggestions that helped improve this paper substantially.

Conflicts of Interest: The authors declare no conflicts of interest.

References

1. Qian, M.G.; Xu, J.L.; Wang, J.C. Further on the sustainable mining of coal. *J. China Coal Soc.* **2018**, *43*, 1–13.
2. Peng, S.P.; Bi, Y.L. Strategic consideration and core technology about environmental ecological restoration in coal mine areas in the Yellow River Basin of China. *J. China Coal Soc.* **2020**, *45*, 1211–1221.
3. Guo, W.B.; Bai, E.H.; Zhao, G.B. Current status and progresson overburden and surface damage and prevention technology of fully mechanized caving mining. *J. China Coal Soc.* **2020**, *45*, 509–523.
4. Guo, W.B. *Damage and Protection in Coal Mining*; Emergency Management Press: Beijing, China, 2019; pp. 1–8.
5. Jing, Y.; Armstrong, R.T.; Mostaghimi, P. Digital coal: Generation of fractured cores with microscale features. *Fuel* **2017**, *207*, 93–101. [CrossRef]
6. Li, Z.; Feng, G.R.; Luo, Y.; Hu, S.Y.; Qi, T.Y.; Jiang, H.N.; Guo, J.; Bai, J.W.; Du, X.J.; Kang, L.X. Multi-tests for pore structure characterization-a case study using lamprophyre. *AIP Adv.* **2017**, *7*, 085204. [CrossRef]
7. Miao, X.X.; Li, S.C.; Chen, Z.Q.; Liu, W.Q. Experimental study of seepage properties crushed sandstone under different porosities. Transp. *Porous Media* **2011**, *86*, 805–814. [CrossRef]
8. Guo, W.B. *Special Mining Technology of Mine*; China University of Mining and Technology Press: Xuzhou, China, 2021; pp. 10–16.
9. Peng, S.S. *Longwall Mining*, 3rd ed.; Taylor & Francis Group: Abingdon, UK, 2019.
10. Qi, C.; Fourie, A. Cemented paste backfill for mineral tailings management: Review and future perspectives. *Miner. Eng.* **2019**, *144*, 106025. [CrossRef]
11. Cacciuttolo, C.; Marinovic, A. Experiences of underground mine backfilling using mine tailings developed in the Andean region of Peru: A green mining solution to reduce socio-environmental impacts. *Sustainability* **2023**, *15*, 12912. [CrossRef]
12. Liu, H.T.; Guo, L.F.; Zhao, X.D. Expansionary evolution characteristics of plastic zone in rock and coal mass ahead of excavation face and the mechanism of coal and gas outburst. *Energies* **2020**, *13*, 984. [CrossRef]
13. Jiang, Q.; Ji, L.J.; Zuo, R.S. Research on mechanism of crushing-compression of coal waste. *J. China Univ. Min. Technol.* **2001**, *30*, 31–34.
14. Ma, Z.G. An experimental study of the compaction of water-saturated over-crushed rock. *Chin. J. Rock Mech. Eng.* **2005**, *24*, 1139–1144.
15. Huang, Y.L.; Zhang, J.X.; Du, J. Time dependence of backfilling body in fully mechanized backfilling mining face. *J. China Univ. Min. Technol.* **2012**, *41*, 697–701.
16. Huang, Y.L. Strata movement control due to bulk factor of backfilling body in fully mechanized backfilling mining face. *J. Min. Saf. Eng.* **2012**, *29*, 162–167.
17. Yang, X.L.; Chu, T.X.; Yu, M.G.; Wang, L.; Chao, J.K.; Han, X.F. Evolution characteristics of bulking factor in the multi-field loading of broken coal: An experimental study. *Rock Mech. Rock Eng.* **2021**, *54*, 1481–1499. [CrossRef]

18. Li, J.M.; Huang, Y.L.; Chen, Z.W.; Zhang, J.X.; Jiang, H.Q.; Zhang, Y.C. Characterizations of macroscopic deformation and particle crushing of crushed gangue particle material under cyclic loading: In solid backfilling coal mining. *Powder Technol.* **2019**, *343*, 159–169. [CrossRef]
19. Yu, B.; Chen, Z.; Ding, Q.; Wang, L. Non-Darcy flow seepage characteristics of saturated broken rocks under compression with lateral constraint. *Int. J. Min. Sci. Technol.* **2016**, *26*, 1145–1151. [CrossRef]
20. Liu, Y.; Dai, F. A damage constitutive model for intermittent jointed rocks under cyclic uniaxial compression. *Int. J. Rock Mech. Min. Sci.* **2018**, *103*, 289–301. [CrossRef]
21. Yang, X.; Liu, E.; Han, X.; Han, X.; Da, W. Experimental Study on Energy Evolution of Sandstone under Uniaxial Cyclic Loading. *Coal Technol.* **2018**, *37*, 21–24.
22. Zhou, Z.; Cai, X.; Li, X.; Cao, W.; Du, X. Dynamic Response and Energy Evolution of Sandstone Under Coupled Static–Dynamic Compression: Insights from Experimental Study into Deep Rock Engineering Applications. *Rock Mech. Rock Eng.* **2020**, *53*, 1305–1331. [CrossRef]
23. Zhang, T.J.; Zhang, L.; Li, S.G.; Liu, J.L.; Pan, H.Y.; Ji, X. Wave Velocity and Power Spectral Density of Hole-Containing Specimens with Different Moisture Content under Uniaxial Compression. *Energies* **2018**, *11*, 3166. [CrossRef]
24. Liu, Y.M.; Liu, H.B.; Mao, H.J. DEM investigation of the effect of intermediate principle stress on particle breakage of granular materials. *Comput. Geotech.* **2017**, *84*, 58–67. [CrossRef]
25. Li, M.; Zhang, J.X.; Zhou, N.; Huang, Y.L. Effect of particle size on the energy evolution of crushed waste rock in coal mines. *Rock Mech. Rock. Eng.* **2017**, *50*, 1347–1354. [CrossRef]
26. Li, M.; Zhang, J.; Gao, R. Compression characteristics of solid wastes as backfill materials. *Adv. Mater. Sci. Eng.* **2016**, *2016*, 2496194. [CrossRef]
27. Zhang, C.; Tu, S.H.; Zhao, Y.X. Compaction characteristics of the caving zone in a longwall goaf: A review. *Environ. Earth Sci.* **2019**, *78*, 27. [CrossRef]
28. Trueman, R. A finite element analysis for the establishment of stress development in a coal mine caved waste. *Min. Sci. Technol.* **1990**, *10*, 247–252. [CrossRef]
29. Zhang, P.F.; Zhang, Y.B.; Zhao, T.B.; Tan, Y.L.; Yu, F.H. Experimental research on deformation characteristics of waste-rock material in underground backfill mining. *Minerals* **2019**, *9*, 102. [CrossRef]
30. Wu, D.T.; Luo, F.; Li, M.; Diao, Y.L.; Guo, Y.J.; Xu, P.D. Macroscopic and microscopic study on the compression bearing characteristics and deformation failure mechanism of gangue with different particle sizes. *Powder Technol.* **2021**, *383*, 198–211. [CrossRef]
31. Wang, Y.; Li, C.H.; Hu, Y.Z. 3D image visualization of meso-structural changes in a bimsoil under uniaxial compression using X-ray computed tomography (CT). *Eng. Geol.* **2019**, *248*, 61–69. [CrossRef]
32. Cheng, Z.; Hu, M.; Wang, J.F. Discrete element modelling of the mechanical behavior of cemented carbonate sand considering the effects of particle shape and breakage. *Chin. J. Comput. Mech.* **2022**, *39*, 315–323.
33. Yang, B.H.; Wu, A.X.; Miao, X.X.; Liu, J.Z. 3D characterization and analysis of pore structure of packed ore particle beds based on computed tomography images. *Trans. Nonferrous Met. Soc. China* **2014**, *24*, 833–838. [CrossRef]
34. Feng, G.R.; Zhang, Y.; Li, Z.; Fang, Z.; Yang, Y.; Yang, X.; Zhang, X. Quantitative analysis of layered re-crushing of crushed coal particles during compression based on CT scanning. *Powder Technol.* **2023**, *426*, 118638. [CrossRef]
35. Dong, L.; Chen, Y.; Sun, D.; Zhang, Y. Implications for rock instability precursors and principal stress direction from rock acoustic experiments. *Int. J. Min. Sci. Technol.* **2021**, *31*, 789–798. [CrossRef]
36. Zou, Q.L.; Ning, Y.; Zhang, B.; Tian, S.; Jiang, Z.; An, Y. Mechanical properties and failure characteristics of sandstone under ramp loading paths. *Geomech. Geophys. Geo-Energy Geo-Resour.* **2023**, *9*, 39. [CrossRef]
37. Qin, R.C.; Zhou, R.; Li, Q.; Lu, C.; Huang, L. Acoustic emission source location method for glass fibre reinforced plastics based on virtual loading focusing enhancement technology. *Nondestruct. Test. Eval.* **2023**, *2023*, 1–16. [CrossRef]
38. Mao, W.; Towhata, I. Monitoring of single-particle fragmentation process under static loading using acoustic emission. *Appl. Acoust.* **2015**, *94*, 39–45. [CrossRef]
39. Michlmayr, G.; Cohen, D.; Or, D. Shear-induced force fluctuations and acoustic emissions in granular material. *J. Geophys. Res. Solid Earth* **2013**, *118*, 6086–6098. [CrossRef]
40. Johnson, P.A.; Ferdowsi, B.; Kaproth, B.M.; Scuderi, M.; Griffa, M.; Carmeliet, J.; Guyer, R.A.; Bas, P.Y.; Trugman, D.T.; Marone, C. Acoustic emission and microslip precursors to stick-slip failure in sheared granular material. *Geophys. Res. Lett.* **2013**, *40*, 5627–5631. [CrossRef]
41. Michlmayr, G.; Or, D. Mechanisms for acoustic emissions generation during granular shearing. *Granul. Matter* **2014**, *16*, 627–640. [CrossRef]
42. Feng, G.R.; Fang, Z.L.; Li, Z.; Qi, T.Y.; Zhao, J.P.; Fan, W.C.; Yang, P.; Yang, X.J.; Yu, Y.R.; Zhang, H.F.; et al. Effect of particle size on re-crushing characteristics of crushed coal during axial loading. *Powder Technol.* **2022**, *407*, 117675.
43. Feng, G.R.; Zhao, J.P.; Wang, H.W.; Li, Z.; Fang, Z.L.; Fan, W.C.; Yang, P.; Yang, X.J. Study of the internal re-breaking characteristics of crushed limestone during compression. *Powder Technol.* **2022**, *396*, 449–455. [CrossRef]
44. Li, J.; Huang, Y.; Chen, Z.; Li, M.; Qiao, M.; Kizil, M. Particle-crushing characteristics and acoustic-emission patterns of crushing gangue backfilling material under cyclic loading. *Minerals* **2018**, *8*, 244. [CrossRef]

45. Li, J.M.; Huang, Y.L.; Zhai, W.; Li, Y.S.; Ouyang, S.Y.; Gao, H.D.; Li, W.; Ma, K.; Wu, L.W. Experimental study on acoustic emission of confined compression of crushed gangue under different loading rates: Disposal of gangue solid waste. *Sustainability* **2020**, *12*, 3911. [CrossRef]
46. Xin, H.Q. Research on deformation and crushing rules and acoustic emission characteristics of gangue bulk under the condition of confined compression. *J. Min. Saf. Eng.* **2020**, *37*, 162–168.
47. Qin, T.; Guo, X.; Huang, Y.; Wu, Z.; Qi, W.; Wang, H. Study on macro-meso deformation law and acoustic emission characteristics of granular gangue under different loading rates. *Minerals* **2022**, *12*, 1422. [CrossRef]
48. Li, W.; Huang, Y.L.; Gao, H.D.; Li, J.M.; Ruan, Z.Y.; Song, T.Q. Study on acoustic emission characteristics of gangue of different graduations during confined compression. *J. Min. Saf. Eng.* **2020**, *37*, 159–165+172.
49. Zhang, J.; Zhu, J.; Huang, W. Crushing and fractal behaviors of quartz sand gravel particles under confined compression. *Chin. J. Geotech. Eng.* **2008**, *30*, 783–787.
50. Wang, Q. *The Pressure-Bearing Characteristics and Deformation Mechanism of Gangue Rib in Gob-Side Entry Retaining by Roof-Fracturing and Pressure-Releasing*; China University of Mining and Technology: Xuzhou, China, 2020.
51. Tyler, S.W.; Wheatcraft, S.W. Fractal scaling of soil particle size distributions: Analysis and limitations. *Soil Sci. Soc. Am. J.* **1992**, *56*, 362–369. [CrossRef]
52. Xu, J.L.; Qin, W.; Chen, X.J.; Hu, G.Z.; Xie, J.L.; Wang, X.Z.; Zhu, W.B. Influencing factors of accumulative effect of overburden strata expansion induced by stress relief. *J. China Coal Soc.* **2022**, *47*, 115–127.

Disclaimer/Publisher's Note: The statements, opinions and data contained in all publications are solely those of the individual author(s) and contributor(s) and not of MDPI and/or the editor(s). MDPI and/or the editor(s) disclaim responsibility for any injury to people or property resulting from any ideas, methods, instructions or products referred to in the content.